FREQUENCY-DOMAIN ACOUSTIC AND ELASTIC MODELING AND WAVEFORM INVERSION IN THE LOGARITHMIC GRID SET

SEUNGWOO CHOI[1], DONG-JOO MIN[1], JU-WON OH[1], WOOKEEN CHUNG[2], WANSOO HA[3] and CHANGSOO SHIN[1]

[1] *Seoul National University, Dept. of Energy Systems Engineering, 1 Gwanak-ro, Gwanak-gu, Seoul 151-744, South Korea. spoppy@snu.ac.kr*
[2] *Korea Maritime University, Dept. of Energy and Resources Engineering, 727 Taejong-ro, Yeongdo-Gu, Busan 606-791, South Korea.*
[3] *Pukyong National University, Dept. of Energy and Resources Engineering, 45 Yongso-ro, Nam-Gu, Busan 608-737, South Korea.*

(Received August 27, 2013; revised version accepted January 18, 2014)

ABSTRACT

Choi, S., Min, D.-J., Oh, J.-W., Chung, W., Ha, W. and Shin, C., 2014. Frequency-domain acoustic and elastic modeling and waveform inversion in the logarithmic grid set. *Journal of Seismic Exploration*, 23: 103-130.

One of the factors influencing the accuracy of the seismic modeling is the boundary condition. Several boundary conditions have been developed and have their own advantages and disadvantages. One possible method to perfectly remove edge reflections is to extend the dimension of a given model so that the edge reflections cannot be recorded within the recording duration. To make this idea feasible without increasing computational costs, we propose acoustic and elastic modeling algorithms performed in the logarithmic grid set, where grid size increases logarithmically from the middle of model surface. This method has an advantage to reduce the number of grids by the property of logarithmic scale. For acoustic and elastic wave modeling in the logarithmic grid set, the wave equations are first converted from the uniform scale to the logarithm scale. Then we apply the conventional node-based finite-difference method for the acoustic case and the cell-based finite-difference method for the elastic case. Numerical examples show that the new modeling algorithms yield solutions comparable to those of the conventional modeling algorithm, although they can suffer from numerical dispersion when the source is located in the coarse grids (far from the origin). Inversion results for the simple layered model and the modified version of the Marmousi-2 model show that the logarithmic inversion algorithms provide results comparable to those obtained by the conventional inversion achieving computational efficiency when the recording duration is not too long and the influence of numerical dispersion is almost negligible in the inversion. We expect that computational efficiency achieved by the logarithmic grid set would be greater in 3D than in 2D.

KEY WORDS: acoustic, elastic, seismic modeling, waveform inversion, logarithmic grid set.

0963-0651/14/$5.00

INTRODUCTION

Seismic modeling, which is a useful tool to describe seismic wave propagation in subsurface media, is also used in seismic inversion and migration. Since seismic modeling is iteratively conducted in seismic inversion and migration, the accuracy and efficiency of seismic inversion and migration depend largely on those of seismic modeling.

Seismic modeling has mainly been performed using the discrete methods such as finite-difference and finite-element methods, where boundary conditions are necessary to suppress the edge reflections arising from finite-sized models unlike real media. Several boundary conditions have been developed. Reynolds (1978), Clayton and Engquist (1977) and Higdon (1991) applied one-way wave equations so that incoming waves cannot be generated and only outgoing waves can propagate through boundaries. Cerjan et al. (1985) and Shin (1995) defined damping areas surrounding a given model, where amplitudes of waves gradually decrease. The perfectly matched layer method (Collino and Tsogka, 2001) eliminates edge reflections in a similar way. These damping methods increase computational costs due to the additional damping areas. However, even though we apply the aforementioned boundary conditions, edge reflections are not perfectly removed. In order not to suffer from edge reflections, we may want to extend the given model so that edge reflections cannot return to receivers within the recording duration. In that case, however, we need a lot of computational efforts. To alleviate computational overburden, the variable grid sets are necessary.

In seismic modeling using the finite-difference or finite-element methods, grid sizes are determined by the maximum frequency and the minimum velocity of given models to minimize numerical dispersions of waves for the entire model as well as by the ability to represent discontinuous structure. In general, as waves propagate through subsurface media, low-frequency components become dominant. In addition, velocities are usually higher in the deeper part than in the shallow part. As a result, grid sizes suitable for low velocity regions near source points may be redundant for regions far from source positions. Based on this feature, non-uniform grid sets have been proposed to reduce computational costs. Moczo (1989) introduced irregular grids whose size is horizontally constant but vertically varying for SH-waves in 2D heterogeneous media. Jastram and Tessmer (1994) used discontinuous grids where the horizontal spacing changes abruptly and vertical spacing becomes gradually coarser on a staggered grid set. Ha and Shin (2012) proposed efficient modeling and inversion techniques using an axis transformation in the Laplace domain.

In this study, we propose a new grid set called 'logarithmic grid set', where grid spacing increases logarithmically with distance from the middle of the surface of a given model and apply it in modeling and inversion algorithms.

Using the logarithmic grid set, we can make edge reflections not recorded within the total recording time, which allows us to efficiently obtain edge-reflection-free modeling results without applying any absorbing or damping boundary condition. In the following sections, we first introduce how the acoustic and elastic wave equations and the source positions in the uniform grid set can be transformed into the logarithmic grid. Next, we verify the modeling operators composed in the logarithmic grid set by comparing them with those composed in the conventional grid set and then apply it to the acoustic and elastic waveform inversion. For waveform inversion, we apply the gradient method based on the adjoint state of modeling operator (e.g., Lailly, 1983; Tarantola, 1984; Pratt et al., 1998) and use the pseudo-Hessian matrix to scale the gradient (Shin et al., 2001). The modeling and inversion algorithms are applied to a simple layered model and a modified version of the Marmousi-2 model (Martin et al., 2006).

ACOUSTIC WAVE EQUATIONS ON THE LOGARITHMIC SCALE

For 2D heterogeneous isotropic media, acoustic wave equation in the frequency domain can be expressed by

$$-(\omega^2/c^2)p = (\partial^2 p/\partial x^2) + (\partial^2 p/\partial z^2) + \delta(x - x_s)\delta(z - z_s)f \quad , \tag{1}$$

where ω is the angular frequency, $c(x,z)$ is the velocity, $p(x,z,\omega)$ is the Fourier-transformed pressure, and f is the source wavelet, respectively. $\delta(x-x_s)$ and $\delta(z - z_s)$ are delta functions locating the source in (x_s, z_s).

To obtain the wave equation on the logarithmic scale, we use the relationship shown in Fig. 1, which can be expressed as follows

$$\chi = g(x) = \mathrm{sgn}(x)\log[1 + x\,\mathrm{sgn}(x)/x_0] \quad , \tag{2}$$

$$\zeta = h(z) = \mathrm{sgn}(z)\log[1 + z\,\mathrm{sgn}(z)/z_0] \quad , \tag{3}$$

where x_0 and z_0 are constants with dimension of distance.

According to the relationships, the differential operators can be changed into

$$\partial p/\partial x = [e^{-\chi \mathrm{sgn}(x)}/x_0](\partial p/\partial \chi) \quad , \tag{4}$$

$$\partial p/\partial z = [e^{-\zeta \mathrm{sgn}(z)}/z_0](\partial p/\partial \zeta) \quad , \tag{5}$$

$$\partial^2 p/\partial x^2 = [e^{-2\chi \mathrm{sgn}(x)}/x_0^2][(\partial^2 p/\partial \chi^2) - \mathrm{sgn}(x)(\partial p/\partial \chi)] \quad , \tag{6}$$

$$\partial^2 p/\partial z^2 = [e^{2\zeta \mathrm{sgn}(z)}/z_0^2][(\partial^2 p/\partial \zeta^2) - \mathrm{sgn}(z)(\partial p/\partial \zeta)] \quad . \tag{7}$$

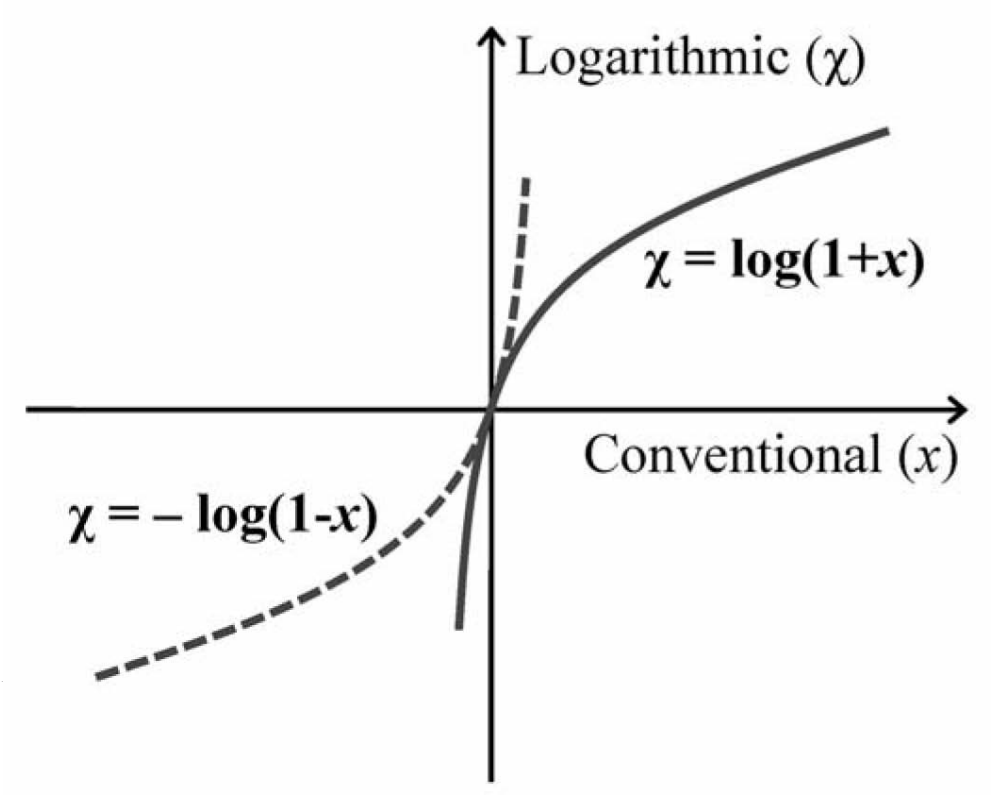

Fig. 1 Diagram showing the relationship between the conventional grid and the logarithmic grid.

The source position can be changed by the intrinsic property of delta function on the logarithmic scale as (Roach, 1982)

$$\delta[g^{-1}(\chi)] = \delta(\chi - \chi_s)/|g^{-1\prime}(\chi_s)| = \delta(\chi - \chi_s)/e^{\chi_s \mathrm{sgn}(x)} , \tag{8}$$

$$\delta[h^{-1}(\zeta)] = \delta(\zeta - \zeta_s)/|h^{-1\prime}(\zeta_s)| = \delta(\zeta - \zeta_s)/e^{\zeta_s \mathrm{sgn}(z)} . \tag{9}$$

Substituting eqs. (6) - (9) into eq. (1) gives the 2D acoustic wave equations on the logarithmic scale as follows

$$\begin{aligned} -(\omega^2/c^2)p = {} & (e^{-2\chi \mathrm{sgn}(z)}/x_0^2)[(\partial^2 p/\partial\chi^2) - \mathrm{sgn}(z)(\partial p/\partial\chi)] \\ & + (e^{-2\zeta \mathrm{sgn}(z)}/z_0^2)[(\partial^2 p/\partial\zeta^2) - \mathrm{sgn}(z)(\partial p/\partial\zeta)] \\ & + [\delta(\chi - \chi_s)/e^{\chi_0 \mathrm{sgn}(x)}][\delta(\zeta - \zeta_s)/e^{\zeta_s \mathrm{sgn}(z)}]f . \end{aligned} \tag{10}$$

ELASTIC WAVE EQUATIONS ON THE LOGARITHMIC SCALE

For 2D heterogeneous isotropic media, the elastic wave equations can be expressed in the frequency domain by

$$\begin{aligned} -\omega^2\rho u = {} & (\partial/\partial x)[(\lambda + 2\mu)(\partial u/\partial x) + \lambda(\partial v/\partial z)] \\ & + (\partial/\partial z)\{\mu[(\partial v/\partial x) + (\partial u/\partial z)]\} \\ & + \delta(x - x_S)\delta(z - z_S)f_x \quad , \end{aligned} \tag{11}$$

$$\begin{aligned} -\omega^2\rho v = {} & (\partial/\partial x)[(\lambda + 2\mu)(\partial v/\partial z) + \lambda(\partial u/\partial x)] \\ & + (\partial/\partial x)\{\mu[(\partial u/\partial z) + (\partial v/\partial x)]\} \\ & + \delta(x - x_S)\delta(z - z_S)f_z \quad , \end{aligned} \tag{12}$$

where $u(x,z,\omega)$ and $v(x,z,\omega)$ are the Fourier-transformed horizontal and vertical displacements, respectively, $\rho(x,z)$ is the density, $\lambda(x,z)$ and $\mu(x,z)$ are the Lamé constants for isotropic media, and f_x and f_z are the horizontal and vertical forces, respectively.

According to eqs. (2) and (3), the differential operators in eqs. (11) and (12) can be expressed on the logarithmic scale as

$$\begin{aligned} & (\partial/\partial x)[k(\partial u/\partial x)] \\ & \quad = (e^{-2\chi sgn(x)}/x_0^2)\{(\partial u/\partial\chi)[k(\partial u/\partial\chi)] - sgn(x)[k(\partial u/\partial\chi)]\} \quad , \end{aligned} \tag{13}$$

$$\begin{aligned} & (\partial/\partial z)[k(\partial u/\partial z)] \\ & \quad = (e^{-2\zeta sgn(z)}/z_0^2)\{(\partial u/\partial\zeta)[k(\partial u/\partial\zeta)] - sgn(z)[k(\partial u/\partial\zeta)]\} \quad , \end{aligned} \tag{14}$$

$$\begin{aligned} & (\partial/\partial x)[k(\partial u/\partial z)] \\ & \quad = (e^{-\chi sgn(x)-\zeta sgn(z)}/x_0z_0)(\partial u/\partial\chi)[k(\partial u/\partial\zeta)] \quad , \end{aligned} \tag{15}$$

$$\begin{aligned} & (\partial/\partial z)[k(\partial u/\partial x)] \\ & \quad = (e^{-\chi sgn(x)-\zeta sgn(z)}/x_0z_0)(\partial u/\partial\zeta)[k(\partial u/\partial\chi)] \quad , \end{aligned} \tag{16}$$

where k represents Lamé constants λ, μ or $\lambda+2\mu$.

Substituting eqs. (8), (9) and (13) - (16) into eqs. (11) and (12) gives the 2D elastic wave equations in the logarithm-scaled coordinate, as follows

$$
\begin{aligned}
-\omega^2\rho u = {} & (e^{-2\chi sgn(x)}/x_0^2)(\partial/\partial\chi)[(\lambda + 2\mu)(\partial u/\partial\chi)] \\
& - sgn(x)(e^{-2\chi sgn(x)}/x_0^2)(\lambda + 2\mu)(\partial u/\partial\chi) \\
& + (e^{-\chi sgn(x)-\zeta sgn(z)}/x_0 z_0)(\partial/\partial\chi)[\lambda(\partial v/\partial\zeta)] \\
& + (e^{-\chi sgn(x)-\zeta sgn(z)}/x_0 z_0)(\partial/\partial\zeta)[\mu(\partial v/\partial\chi)] \\
& + (e^{-2\zeta sgn(z)}/z_0^2)(\partial/\partial\zeta)[\mu(\partial u/\partial\zeta)] \\
& - sgn(z)(e^{-2\zeta sgn(z)}/z_0^2)\mu(\partial u/\partial\zeta) \\
& + [\delta(\chi - \chi_s)/e^{\chi_s sgn(x)}][\delta(\zeta - \zeta_s)/e^{\zeta_0 sgn(z)}] \ , \qquad (17)
\end{aligned}
$$

$$
\begin{aligned}
-\omega^2\rho v = {} & (e^{-2\zeta sgn(z)}/z_0^2)(\partial/\partial\zeta)[(\lambda + 2\mu)(\partial v/\partial\zeta)] \\
& - sgn(x)(e^{-2\zeta sgn(z)}/z_0^2)(\lambda + 2\mu)(\partial v/\partial\zeta) \\
& + (e^{-\chi sgn(x)-\zeta sgn(z)}/x_0 z_0)(\partial/\partial\zeta)[\lambda(\partial u/\partial\chi)] \\
& + (e^{-\chi sgn(x)-\zeta sgn(z)}/x_0 z_0)(\partial/\partial\chi)[\mu(\partial u/\partial\zeta)] \\
& + (e^{-2\chi sgn(x)}/x_0^2)(\partial/\partial\chi)[\mu(\partial v/\partial\chi)] \\
& - sgn(x)(e^{-2\chi sgn(x)}/x_0^2)\mu(\partial v/\partial\chi) \\
& + [\delta(\chi - \chi_s)/e^{\chi_0 sgn(x)}][\delta(\zeta - \zeta_s)/e^{\zeta_0 sgn(z)}] \ . \qquad (18)
\end{aligned}
$$

MODELING AND INVERSION ALGORITHMS ON THE LOGARITHMIC SCALE

Modeling

For acoustic modeling, we need to discretize the modified acoustic wave equations, i.e., eq. (10). We adopt the conventional finite-difference method for acoustic modeling. For elastic modeling, we also use the finite-difference method that only uses displacements rather than the staggered grid methods. In order to properly describe the stress-free boundary conditions at the free surface, we employ the cell-based finite-difference method (Min et al., 2004), where material properties are defined within the area rather than at the nodes. We do not apply any boundary conditions to remove edge reflections. In both acoustic and elastic forward modelling for a wave equation in the frequency domain, the difference equation can be written in a matrix form as

$$\mathbf{Su} = \mathbf{f} \quad , \tag{19}$$

where **S** is the complex impedance, and **u** and **f** are the displacement and source vectors, respectively.

Inversion

For acoustic and elastic waveform inversion, we build objective functions based on the l_2-norm of residuals between model responses and observed data, and minimize the objective function using the gradient method. For simplicity, if we consider the monochromatic data recorded for one shot, the objective function can be expressed as

$$E = \tfrac{1}{2} \| \mathbf{u} - \mathbf{d} \| \quad , \tag{20}$$

where **u** and **d** are the model responses and observed data, respectively. The gradient direction can be obtained by taking partial derivatives of eq. (20) with respect to the parameters. The gradient with respect to the kth parameter can be written by

$$\partial E/\partial m_k = \mathrm{Re}\{(\partial \mathbf{u}/\partial m_k)^T(\mathbf{u} - \mathbf{d})^*\} \quad , \tag{21}$$

where the superscripts T and * indicate the transpose and the complex conjugate, respectively. The partial derivative wavefield can be computed from the matrix equation [eq. (19)] for forward modeling. Taking eq. (19) with respect to the kth model parameter yields

$$\mathbf{S}(\partial \mathbf{u}/\partial m_k) = -(\partial \mathbf{S}/\partial m_k)\mathbf{u} = \mathbf{f}_v^{(k)} \quad , \tag{22}$$

$$\partial \mathbf{u}/\partial m_k = \mathbf{S}^{-1}\mathbf{f}_v^{(k)} \quad , \tag{23}$$

where $\mathbf{f}_v^{(k)}$ is the virtual source vector for the k-th parameter. Substituting eq. (23) into eq. (21) gives

$$\partial E/\partial m_k = \mathrm{Re}\{[\mathbf{f}_v^{(k)}]^T(S^{-1})^T(\mathbf{u} - \mathbf{d})^*\} \quad . \tag{24}$$

For the entire model parameter, the gradient can be rewritten by

$$\partial E/\partial \mathbf{m} = \mathrm{Re}\{(\mathbf{F}_v)^T(S^{-1})^T(\mathbf{u} - \mathbf{d})^*\} \quad , \tag{25}$$

where **m** is the model parameter vector, and $\mathbf{F}_v$ is the virtual source matrix. Note that **S** is asymmetric in the logarithmic grid set unlike in the conventional grid set, which gives different solutions when we switch source and receiver

positions to check the reciprocity theorem. While the phase of solution is the same, the amplitude is scaled by the scaling factors for source positions expressed in eqs. (8) and (9). Because $(S^{-1})^T$ means that the source and receiver positions are switched, the scaling factors in eqs. (8) and (9), which are supposed to be applied to source positions, should be applied to solutions at receivers to compute $(S^{-1})^T(\mathbf{u} - \mathbf{d})^*$. This process does not require additional computing memory.

To obtain the gradient for all the sources and frequencies, the gradients for one source and one frequency, eq. (24), are summed and scaled over shots and frequencies as follows (Ha et al., 2009),

$$\nabla E = \mathrm{NRM}\Big\{ \sum_{f} (\mathrm{NRM}[\{ \sum_{s} \mathrm{diag}(\mathbf{F}_v^T\mathbf{F}_v^*) + \beta\mathbf{I}\}^{-1}[\sum_{s} (\partial E/\partial \mathbf{m})]]) \Big\} \quad , \quad (24)$$

where $\mathbf{I}$ is the identity matrix, s and f indicate source and frequency, respectively, and NRM indicates the normalization operator. Gradient is scaled by the diagonal of the pseudo-Hessian matrix (Shin et al., 2001), which is computed by the square of virtual source matrix ($\mathbf{F}_v^T\mathbf{F}_v^*$). To avoid the ill-condition or singularity of the pseudo-Hessian matrix, the damping factor β is added to the diagonal elements. Next, the gradient vector at each frequency is normalized with its largest absolute value and summed over all frequencies. This resultant gradient is normalized once again.

We also apply the modified version (Ha et al., 2009) of the conjugate gradient method (Fletcher and Reeves, 1964). The conjugate gradient direction $\mathbf{g}$ is obtained by

$$\mathbf{g}^{(1)} = -\nabla E^{(1)} \quad , \quad (25)$$

$$\mathbf{g}^{(n)} = -\nabla E^{(n)} + \{[(\nabla E^{(n)})^T\nabla E^{(n)}]/[(\nabla E^{(n-1)})^T\nabla E^{(n-1)}]\}\mathrm{NRM}[\mathbf{g}^{(n-1)} \quad , \quad (26)$$

where the superscript (n) is the iteration number. The normalized conjugate gradient direction obtained in the previous iteration is used to compute the conjugate gradient direction at the present iteration. Consequently, the model parameter vector is updated by

$$\mathbf{m}^{(n+1)} = \mathbf{m}^{(n)} + \alpha\mathbf{g}^{(n)} \quad , \quad (27)$$

where α is the step length.

NUMERICAL EXAMPLES

The modeling and inversion algorithms composed on the logarithmic scale are demonstrated for the modified version of the Marmousi-2 model. The model on the uniform scale is shown in Fig. 2a, and Fig. 2b shows the model on the logarithmic scale. The modified version of the Marmousi-2 model is obtained removing the water layer and the parts of the left- and right-hand sides. The dimension of the modified version is 9 km in width and 3.02 km in depth. Poisson's ratio and density are fixed at 0.25 and 2 g/cm^3, respectively.

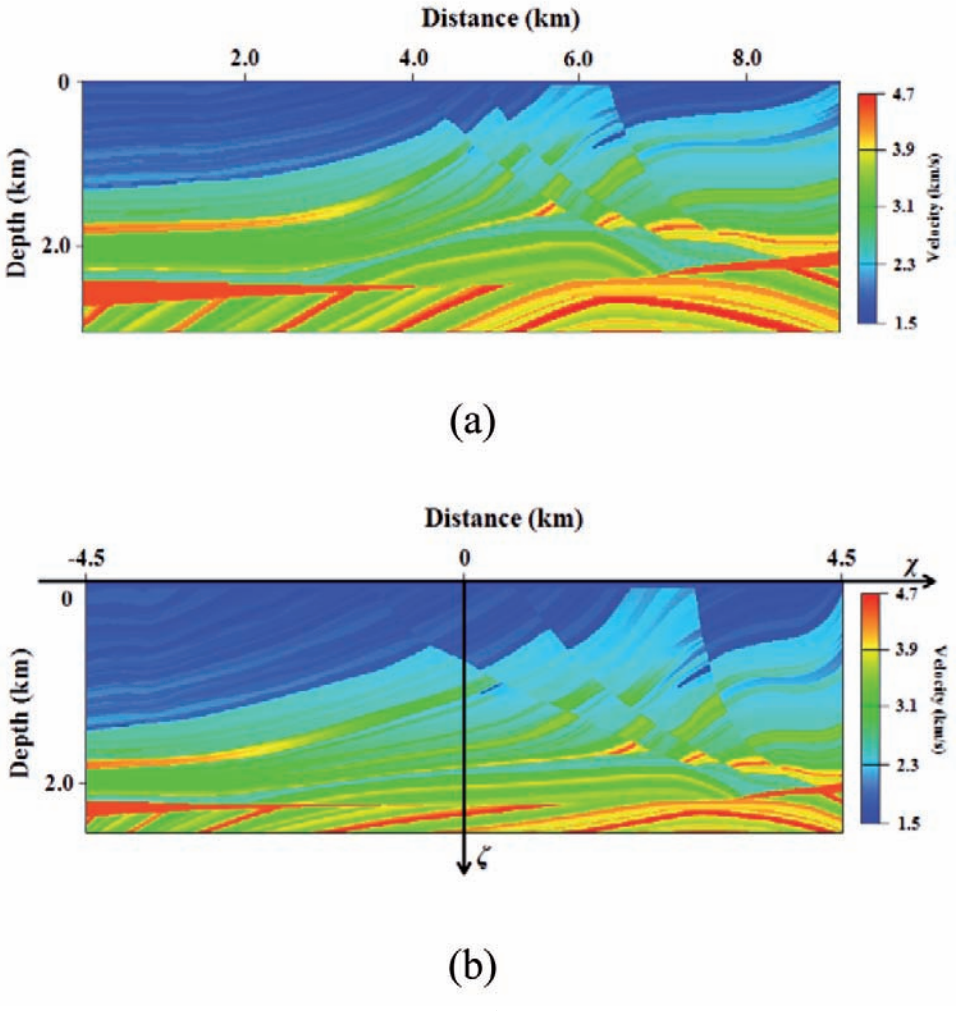

Fig. 2. P-wave velocity models for the modified version of Marmousi-2 model on the (a) conventional uniform and (b) logarithmic scales.

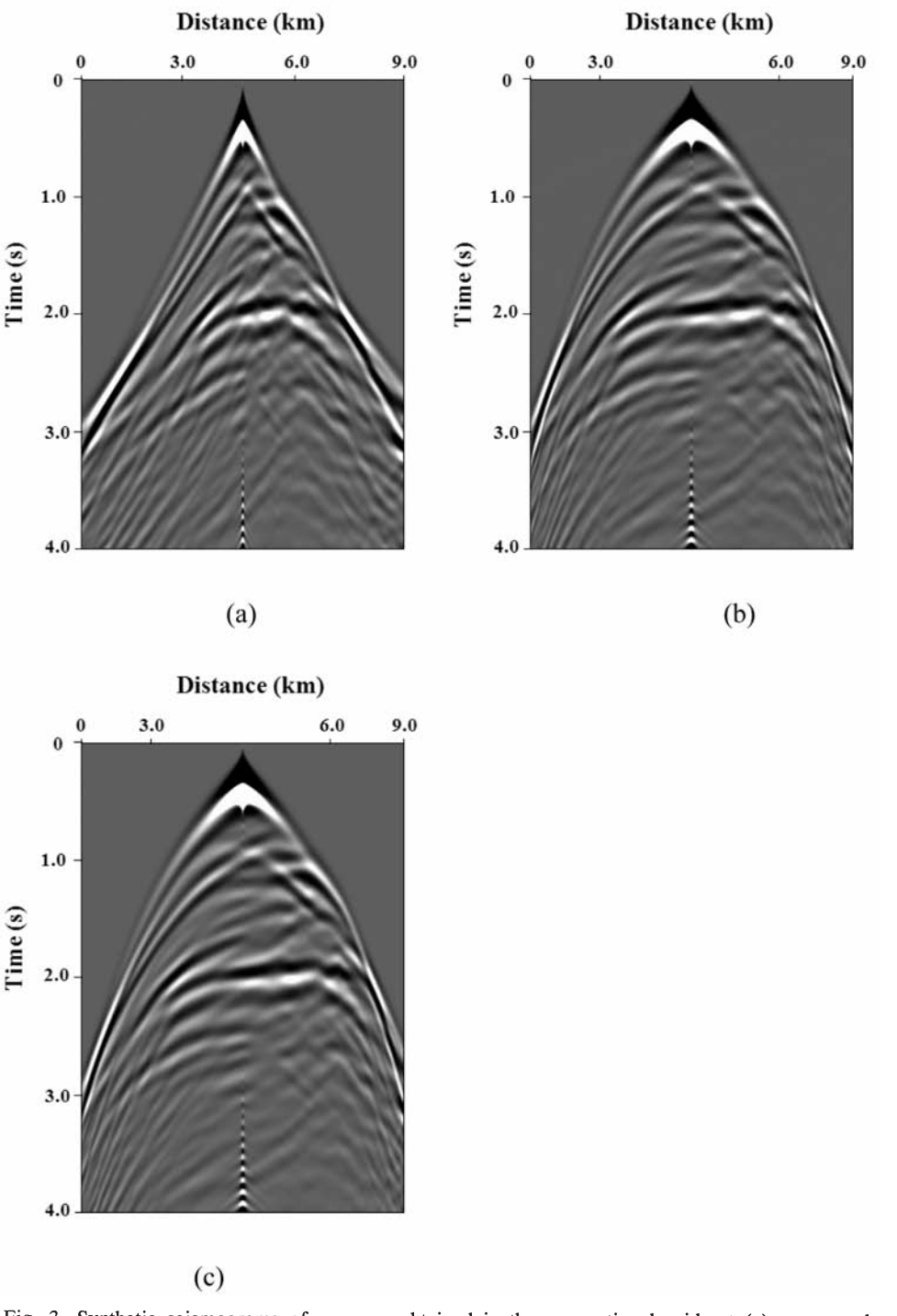

Fig. 3. Synthetic seismograms of pressure obtained in the conventional grid set (a), converted through interpolation from the conventional to the logarithmic grid set (b) and obtained in the logarithmic grid set (c).

Modeling results

We first verify the modeling results obtained in the logarithmic grid set by comparing them with those obtained in the conventional grid set. Particularly, the accuracy of the new elastic modelling algorithm was demonstrated for Lamb's problem in Appendix A. In the logarithmic grid set, because of the nature of the logarithmic scale, the same-sized model can be simulated with fewer grid points than in the conventional grid set. Therefore, it is easy to extend the given model so that edge reflections cannot be recorded at receivers within the recording duration. For the conventional grid set, the PML boundary condition is applied to remove edge reflections, whereas in the logarithmic grid set, we do not use any boundary conditions but extend the model for boundary areas. In both the conventional and logarithmic grid sets, we use 50 additional grids for boundary areas. Grid size is 10 m for acoustic wave modeling and 5 m for elastic wave modeling. When grid space is 10 m, the total number of grids is 1001 in width and 353 in depth in the conventional grid set, whereas the number of grids is 441 in width and 190 in depth in the logarithmic grid set. In elastic case, the total number of grids is 1901 by 657 in the conventional grid set, whereas the number of grids is 783 by 330 in the logarithmic grid set. For source wavelet, the first derivative of the Gaussian function whose maximum frequency is 10 Hz is used and the maximum recording time is 4 s. Fig. 3 shows seismograms of pressure in the conventional and logarithmic grid sets. In Fig. 4, we compare single traces obtained in both grid sets with each other. In Figs. 5 and 6, we display elastic modeling results. These results demonstrate that the modeling results obtained in the logarithmic grid set are compatible with those obtained in the conventional grid set and the interpolation is properly applied.

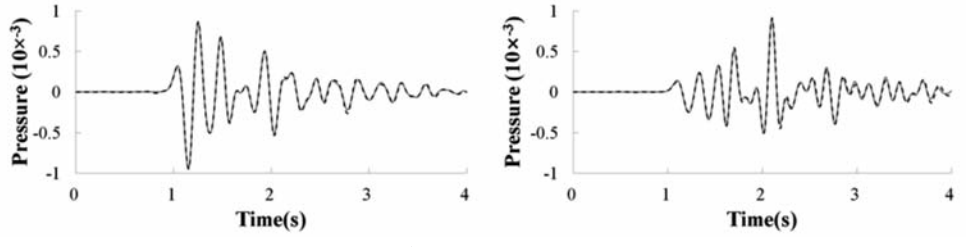

Fig. 4. Comparison of traces extracted at distances of 3.15 km and 5.85 km of the seismograms for pressure (Fig. 3) obtained in the conventional (solid line) and logarithmic (dashed line) grid sets.

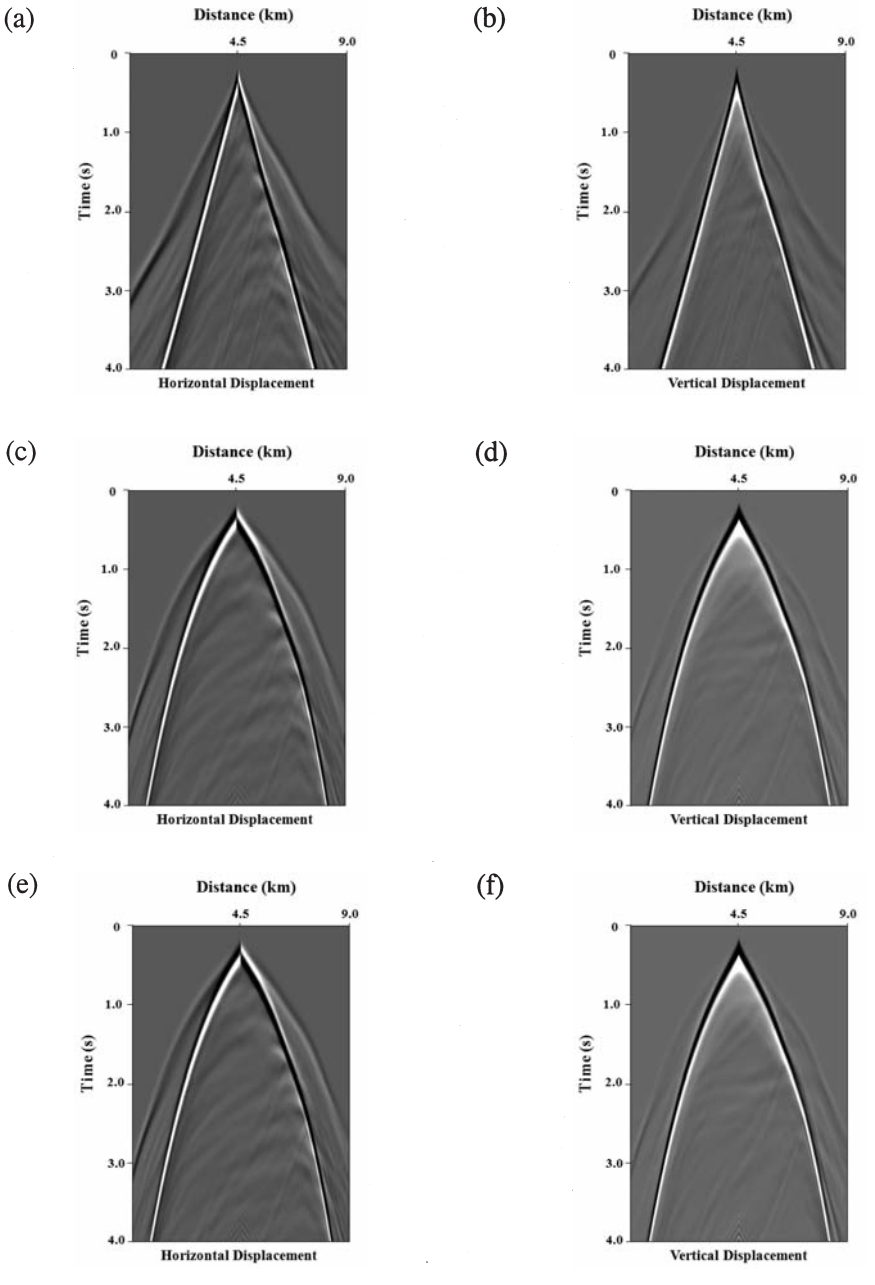

Fig. 5. Synthetic seismograms of horizontal (left) and vertical (right) displacements obtained in the conventional grid set (a, b), converted through interpolation from the conventional to the logarithmic grid set (c, d) and obtained in the logarithmic grid set (e, f).

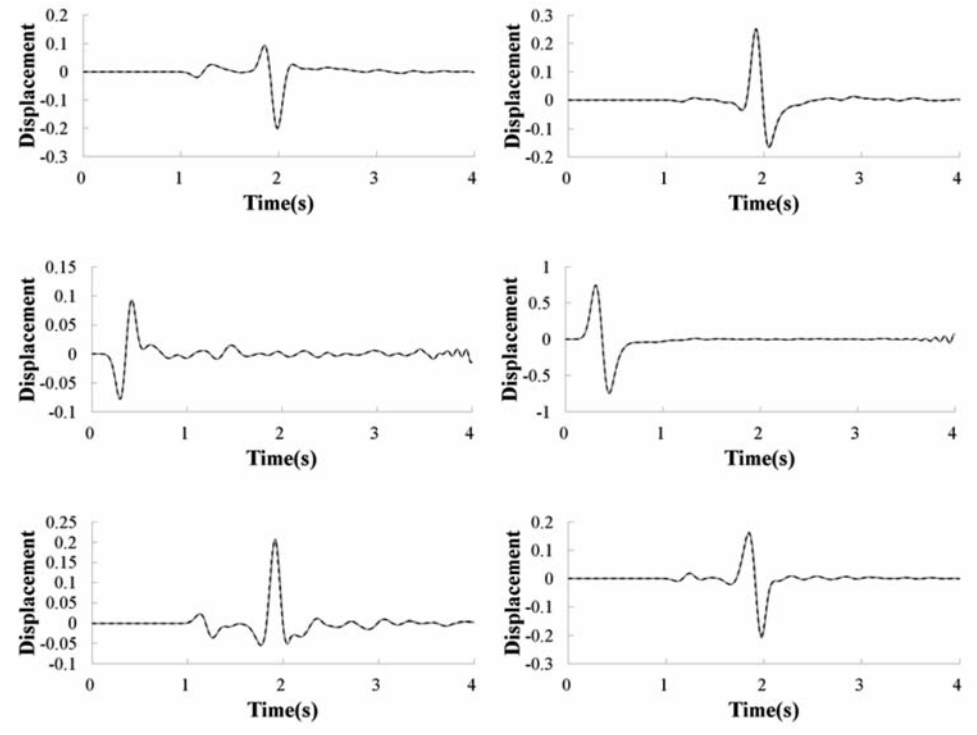

Fig. 6. Comparison of traces extracted at distances of 3.15 km, 4.5 km and 5.85 km of the seismograms for horizontal (left) and vertical (right) displacements (Fig. 5) obtained in the conventional (solid line) and logarithmic (dashed line) grid sets.

Inversion results

We perform the acoustic waveform inversion in the logarithmic grid set. We first use the simple model shown in Fig. 7a, where the high-velocity layer exists in the middle of the model. The dimension of the model is 4 km by 2 km. We apply the inversion algorithms in the conventional and logarithmic grid sets to the same synthetic data generated in the conventional grid set with PML boundary condition. The maximum recording time is 3 s. We assume that 399 shot gathers are acquired with the interval of 10 m for field data. For the inversion in the logarithmic grid set, the field data should be transformed to the logarithmic grid set through interpolation. For initial guesses, the linearly increasing velocity model ($1.5 \leq 4.5$ km/s) is used for the conventional method, whereas the exponentially increasing velocity model is employed for the logarithmic inversion.

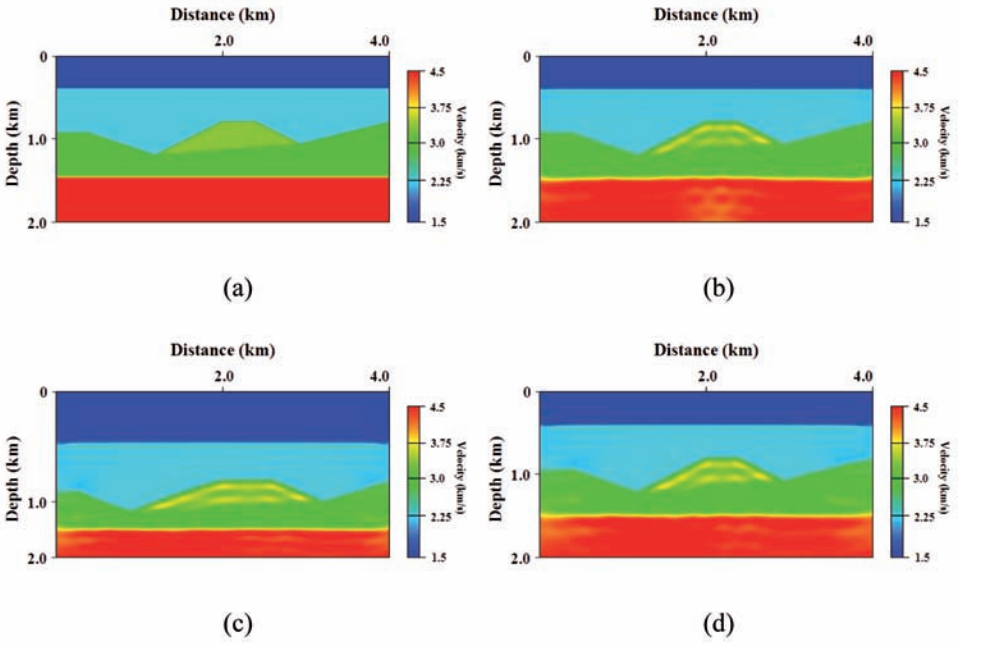

Fig. 7. (a) True simple layered velocity model and inversion results obtained at the 200th iteration by using the (b) conventional and (c) logarithmic grid sets. For comparison, the logarithmic inversion result (c) is converted to the conventional grid set in (d).

Figs. 7b and 7c show the models inverted at the 200th iteration in the conventional and logarithmic grid sets. For comparison, the model inverted in the logarithmic grid set is converted to the conventional grid set through interpolation (Fig. 7d). In Fig. 7, we observe that the logarithmic inversion yields results comparable to those obtained by the conventional inversion. In Fig. 8, we display depth profiles extracted in the middle of the inverted velocity models of Figs. 7b and 7d as well as the true velocity model. Fig. 8 shows that both the conventional and logarithmic inversion algorithms give reliable solutions. However, the resolution of the logarithmic inversion is not as good as that of the conventional inversion for deeper part, which may be because of the logarithmically increasing grid interval in the logarithmic grid set.

We proceed to perform the inversion for the synthetic data generated in the conventional grid set for the modified version of the Marmousi-2 model (Fig. 2a) for both acoustic and elastic cases. We apply both the conventional and logarithmic inversion algorithms to the same synthetic data generated in the conventional grid set with PML boundary condition.

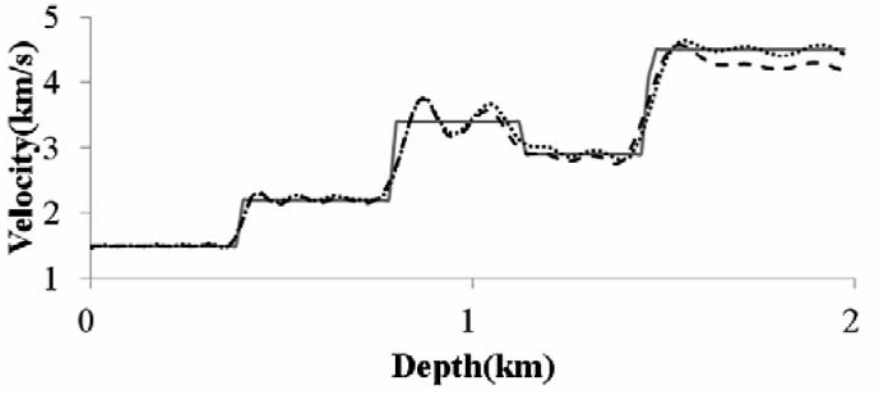

Fig. 8. Depth profiles at the center of the true velocity model (solid line) and the inverted velocity models generated in the conventional (dotted line) and logarithmic (dashed line) grid sets.

For acoustic waveform inversion, the maximum recording time is 4 s. We assume that 899 shot gathers are acquired with the interval of 10 m for field data. For the inversion in the logarithmic grid set, the field data should be transformed to the logarithmic grid set through interpolation. Figs. 9a and 9b show models inverted at the 200th iteration using the conventional and logarithmic grid sets, respectively. For comparison, we also convert the model inverted in the logarithmic grid set to the conventional grid set through interpolation. Fig. 10 shows depth profiles extracted from the inverted velocity models of Figs. 9a and 9c as well as the true velocity model. In Fig. 10, it is observed that velocities inverted by using the conventional and logarithmic grid sets are compatible with the true velocities.

We compare the computing time required to perform acoustic waveform inversion in the conventional and logarithmic grid sets. Table 1 shows CPU times taken to iterate inversion process 200 times for the simple layered model and the Marmousi-2 model using 20 Intel Xeon E5640 2.66 GHz CPUs on the Linux-cluster machine. This indicates that it is more efficient to use the logarithmic grid, because we can reduce the number of grids.

Table 1. CPU times required to perform the acoustic inversion for the simple layered model and the Marmousi-2 model for 200th iteration.

Model	Conventional grid set	Logarithmic grid set	Ratio (C/L)
Simple layered model	18330.65815	6323.366236	2.9
Marmousi-2 model	112242.7616	22074.23556	5.1

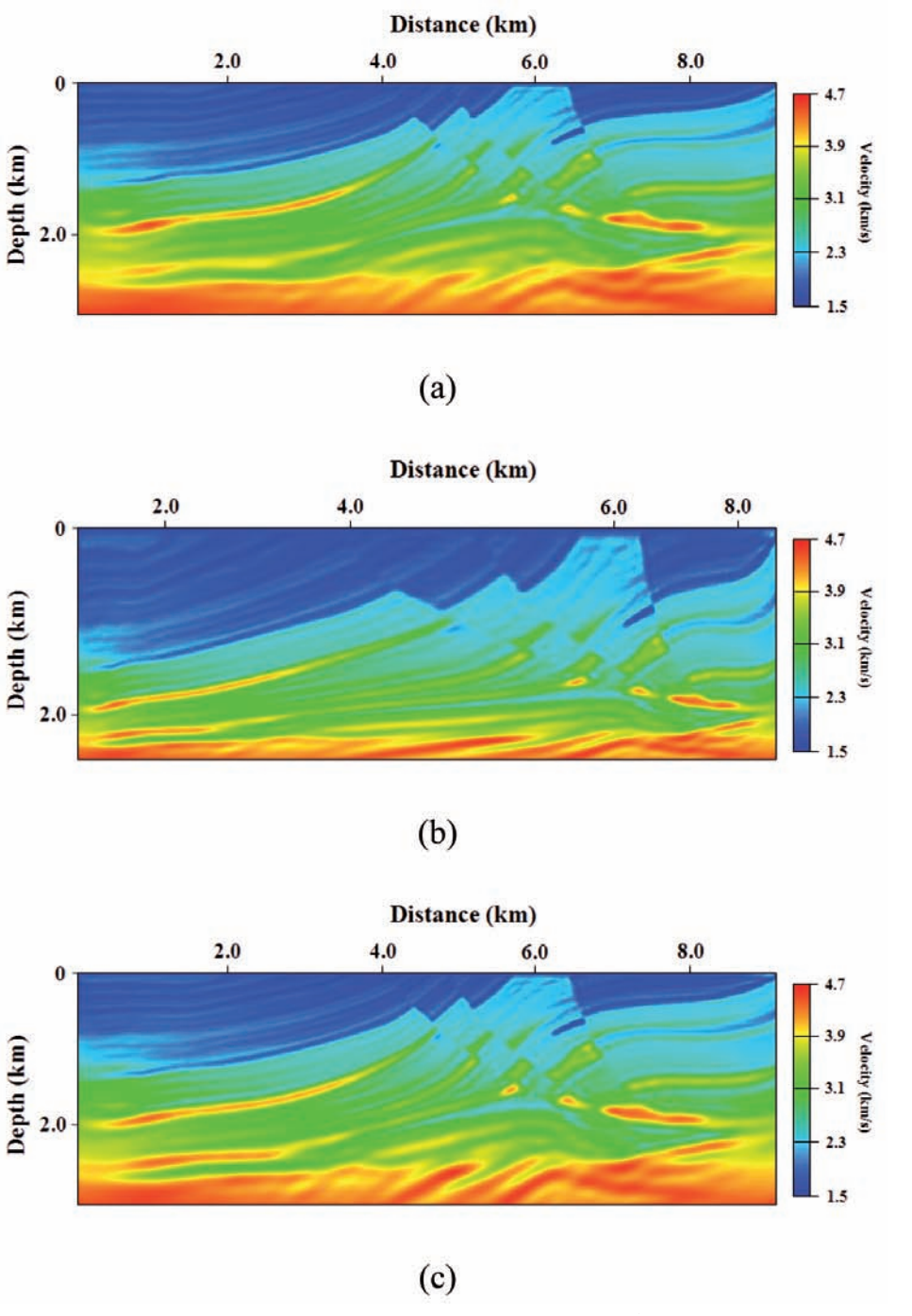

Fig. 9. Inversion results obtained at the 200th iteration by using the (a) conventional and (b) logarithmic grid sets. For comparison, the logarithmic inversion result (b) is converted to the conventional grid set in (c).

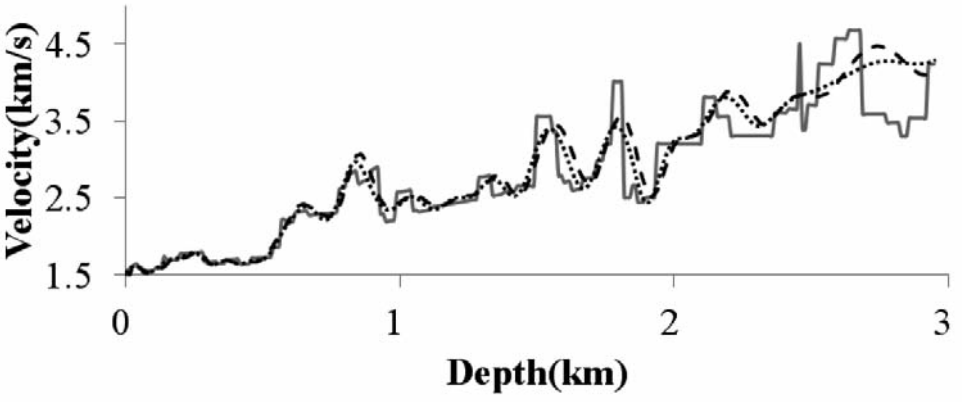

(a)

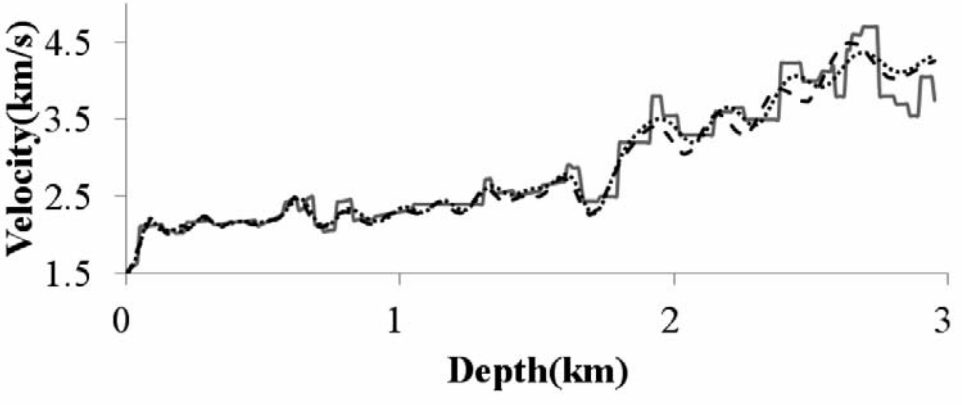

(b)

Fig. 10. Depth profiles at distances of (a) 4.5 km and (b) 6 km of the true velocity model (solid line) and the inverted velocity models generated in the conventional (dotted line) and logarithmic (dashed line) grid sets.

However, when the recording time increases, the boundary area of the model should also increase. If the recording duration is too long compared to the model dimension, the logarithmic inversion becomes less efficient than the conventional inversion. We may conclude that the efficiency of the waveform inversion in the logarithmic grid set is dependent on the recording time.

For the elastic waveform inversion, the maximum recording time is 5 s and we use 898 shot gathers for field data. In the elastic case, the frequency marching method (Bunks et al., 1995) is also employed over 5 stages: 0.2 ~ 2 Hz, 0.2 ~ 4 Hz, 0.2 ~ 6 Hz, 0.2 ~ 8 Hz, 0.2 ~ 10 Hz. For each frequency group, the inversion process is repeated for 30 iterations. Fig. 11a shows the inverted model for P-wave velocity in the logarithmic set. Through interpolation, the inverted model on the logarithm scale is converted to the conventional grid set (Fig. 11b). Fig. 12 shows depth profiles extracted from the true and inverted P-wave velocity models for quantitative comparison. Figs. 11b and 12 indicate that inversion results obtained by the new elastic waveform inversion method are comparable to true values.

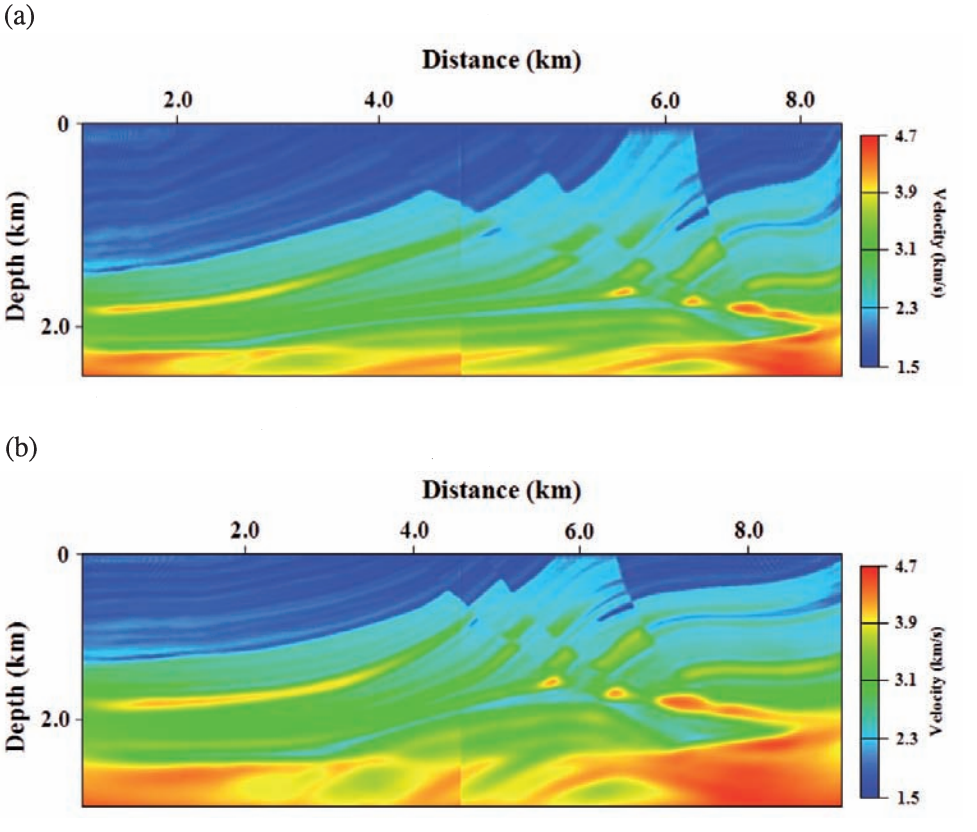

Fig. 11. (a) P-wave velocity models inverted at the 200th iteration in the logarithmic grid set for the modified version of the Marmousi-2 model and (b) its interpolated version to the conventional grid set.

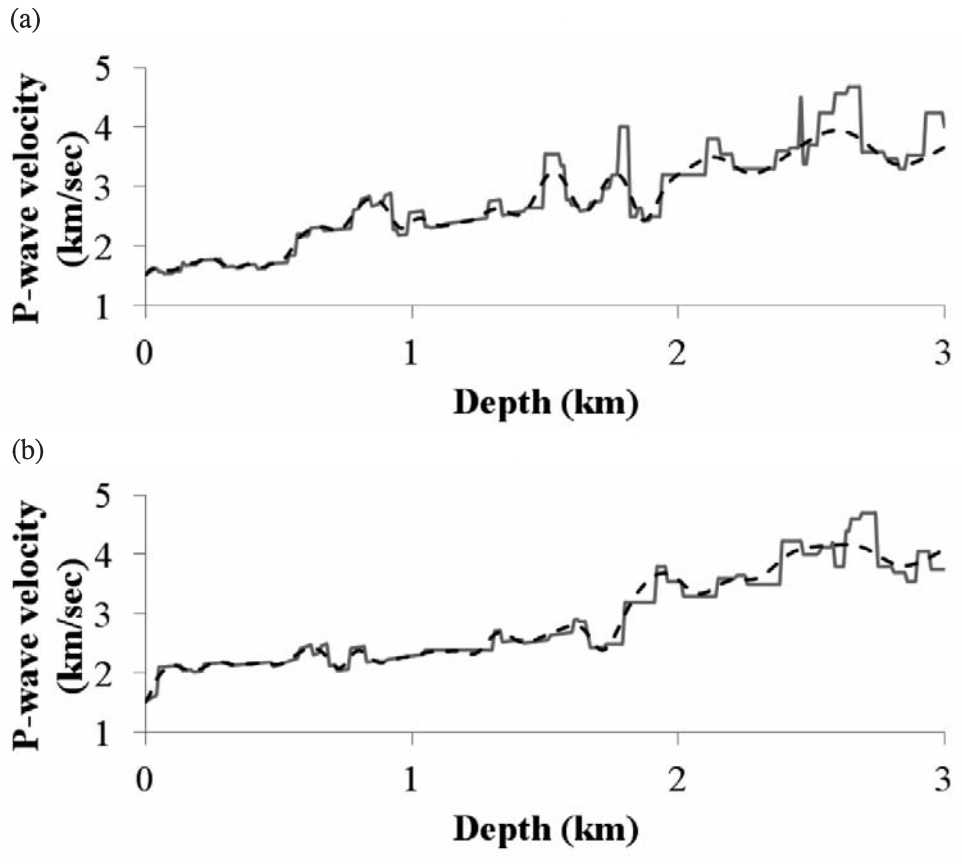

Fig. 12. Depth profiles at distances of (a) 4.5 km and (b) 6 km of the true velocity model (solid line) and the inverted velocity models.

CONCLUSIONS

We developed new acoustic and elastic wave modeling and waveform inversion algorithms, which are performed in the logarithmic grid set. In the logarithmic grid set, since the grid interval increases logarithmically with distance, we require fewer grid points than in the conventional uniform grid set. Based on this feature, we can extend the given model without increasing computational efforts compared to the conventional method, so that edge reflections cannot be recorded at receivers within the recording duration. Since the number of additional grids used to extend the given model can be determined considering the recording duration, the efficiency of the new modeling and inversion algorithms is mainly dependent on the recording duration.

In order to apply the new modeling and inversion algorithms in the logarithmic grid set, interpolation is needed. Field data acquired in the conventional uniform grid should be converted to the logarithmic grid set, and inversion results on the logarithmic scale need to be converted to the conventional uniform grid set. The new modeling algorithm yielded numerical solutions compatible with analytic solutions. However, we need to know that when the source is applied near the boundary of the given model where the grid interval is large, the seismograms can suffer from numerical dispersion. We examined if the numerical dispersion is serious in waveform inversion or not. Inversion results for the simple layered model showed that the logarithmic waveform inversion yields results comparable to those obtained by the conventional waveform inversion. By comparing the inversion results obtained by the logarithmic waveform inversion with those of the conventional method for the modified version of the Marmousi-2 model, we showed that the new logarithmic waveform inversion can be applied to the complicated model with computation efficiency. From all the inversion results, we noted that numerical dispersion does not seriously influence inversion results. The frequency marching method may contribute to reducing the influences of numerical dispersion in high frequencies. Although we only test the new modeling and inversion algorithms to 2D problems, their efficiency will be greater in 3D problems. We also feel that the new modeling and inversion methods may contribute to improving the efficiency of data acquisition.

ACKNOWLEDGMENTS

This work was supported financially by the Human Resources Development (No. 20124010203200), the "Development of Technology for CO_2 Marine Geological Storage" funded by the Ministry of Oceans and Fisheries, Korea, and the Korea CCS R&D Center (KCRC) grant funded by the Korea government Ministry of Science, ICT & Future Planning (No. 2012-0008926).

REFERENCES

Bunks, C., Saleck, F.M., Zaleski, S. and Chavent, G., 1995. Multiscale seismic waveform inversion. Geophysics, 60: 1457-1473.

Cerjan, C., Kosloff, D., Kosloff, R. and Reshef, M., 1985. A nonreflecting boundary condition for discrete acoustic and elastic wave equation. Geophysics, 50: 705-708.

Clayton, R. and Enquist, B., 1977. Absorbing boundary conditions for acoustic and elastic wave equations. Bull. Seismol. Soc. Am., 67: 1529-1540.

Collino, F. and Tsogka, C., 2001. Application of the PML absorbing layer model to the linear elastodynamic problem in anisotropic heterogeneous media. Geophysics, 66: 294-307.

Ewing, W.M., Jardetzky, W.S. and Press, F., 1957. Elastic Waves in Layered Media. McGraw-Hill Inc., New York.

Fletcher, R. and Reeves, C.M., 1964. Function minimization by conjugate gradient. The Comput. J., 7: 149-154.

Ha, W. and Shin, C., 2012. Efficient Laplace-domain modeling and inversion using an axis transformation technique. Geophysics, 77: R141-R148.

Ha, T., Chung, W. and Shin, C., 2009. Waveform inversion using a back-propagation algorithm and a Huber function. Geophysics, 74(3): R15-R24.

Higdon, R.L., 1991. Absorbing boundary conditions for elastic waves. Geophysics, 56: 231-241.

Jastram, C. and Tessmer, E., 1994. Elastic modeling on a grid with vertically varying spacing. Geophys. Prosp., 42: 357-370.

Lailly, P., 1983. The seismic inverse problem as a sequence of before stack migration. In: Bednar, J.B., Rednar, R., Robinson, E.A. and Weglein, A.B. (Eds.), Conf. on Inverse Scattering: Theory and Application. Soc. Industr. Appl. Mathem.: 206-220.

Martin, G.S., Wiley, R. and Marfurt, K.J., 2006. Marmousi2: An elastic upgrade for Marmousi. The Leading Edge, 25: 156-166.

Min, D.-J., Shin, C. and Yoo, H.S., 2004. Free-surface boundary condition in finite-difference elastic wave modeling. Bull. Seismol. Soc. Am., 94: 237-250.

Moczo, P., 1989. Finite-difference technique for SH waves in 2-D media using irregular grids: application to the seismic response problem. Geophys. J. Internat., 99: 321-329.

Pratt, R.G., Shin, C. and Hicks, G.J., 1998. Gauss-Newton and full Newton methods in frequency-space seismic waveform inversion. Geophys. J. Internat., 133: 341-362.

Reynolds, A.C., 1978. Boundary conditions for the numerical solution of wave propagation problems. Geophysics, 43: 1099-1110.

Roach, G.F., 1982. Green's Functions (2nd ed.). Cambridge University Press, Cambridge.

Shin, C., 1995. Sponge boundary condition for frequency-domain modeling. Geophysics, 60: 1870-1874.

Shin, C., Jang, S. and Min, D.-J., 2001. Improved amplitude preservation for prestack depth migration by inverse scattering theory. Geophys. Prosp., 49: 592-606.

Tarantola, A., 1984. Inversion of seismic reflection data in the acoustic approximation. Geophysics, 49: 1259-1266.

APPENDIX A

COMPARISON OF NUMERICAL SOLUTIONS WITH ANALYTIC SOLUTIONS

In order to investigate the accuracy of the elastic modeling algorithm in the logarithmic grid set, we need to compare numerical solutions with analytic solutions for Lamb's problem, for which we assume the semi-infinite homogeneous model shown in Fig. A-1. We compute analytic solutions referring to Ewing et al. (1957). We first compute analytic solutions in the frequency-wavenumber domain, and then take their inverse Fourier transform to obtain solutions in the time-space domain. Solutions in the logarithmic grid set are obtained through interpolation. Fig. A-2 shows analytic solutions and numerical solutions obtained in the logarithmic grid set. From Fig. A-2, we see that numerical solutions agree well with analytic solutions.

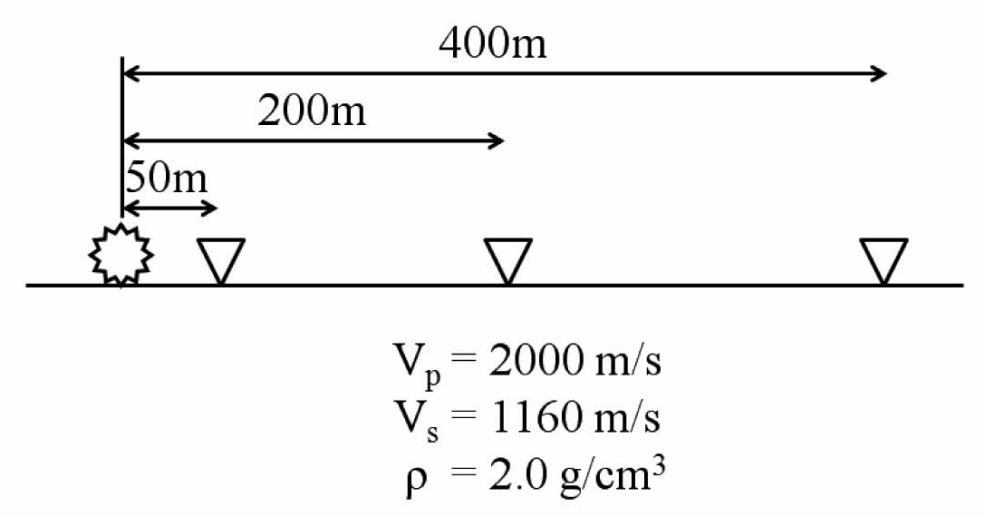

Fig. A-1. The geometry of the semi-infinite homogeneous model for Lamb's problem.

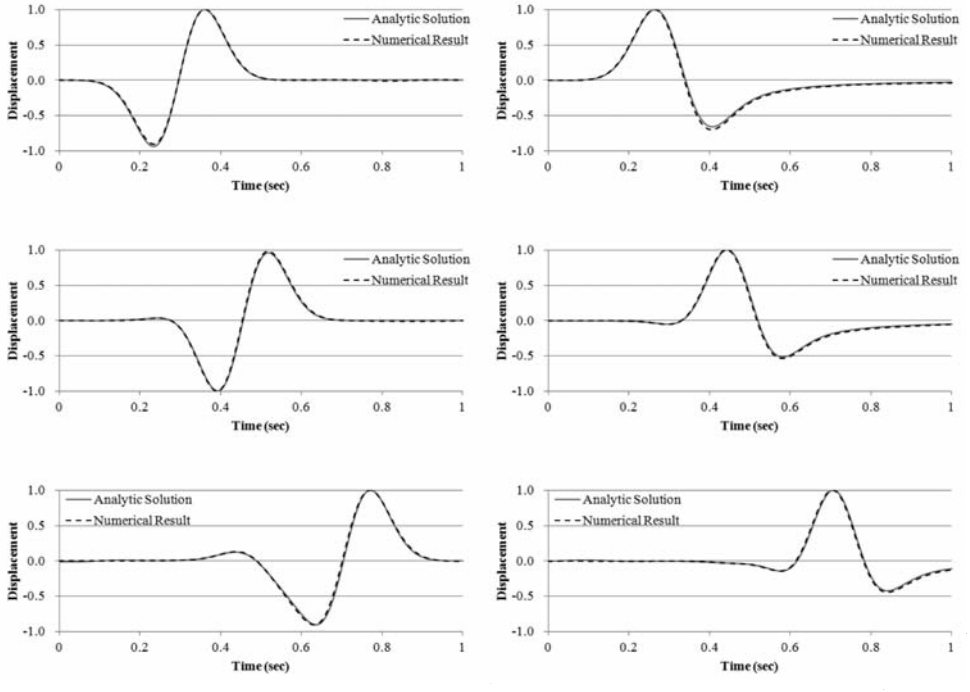

Fig. A-2. Horizontal (left) and vertical displacements (right) of analytic (solid line) and numerical solutions obtained in the logarithmic grid set (dashed line) at distances of 50, 200 and 400 m from the source point.

APPENDIX B

DISPERSION CURVES

We compute numerical phase velocity curves for dispersion analysis in the logarithmic grid sets. We begin with eq. (1) discarding the source term. Uniform grids in the logarithmic scale correspond to the exponentially increasing grids in the uniform scale (Fig. B-1). If we assume that the grid interval in the logarithmic grid set is constant as "a", the grid interval increases by "e^a" in the conventional grid set as shown in Fig. B-1. Numerical phase velocities are computed for the exponentially increasing grid set.

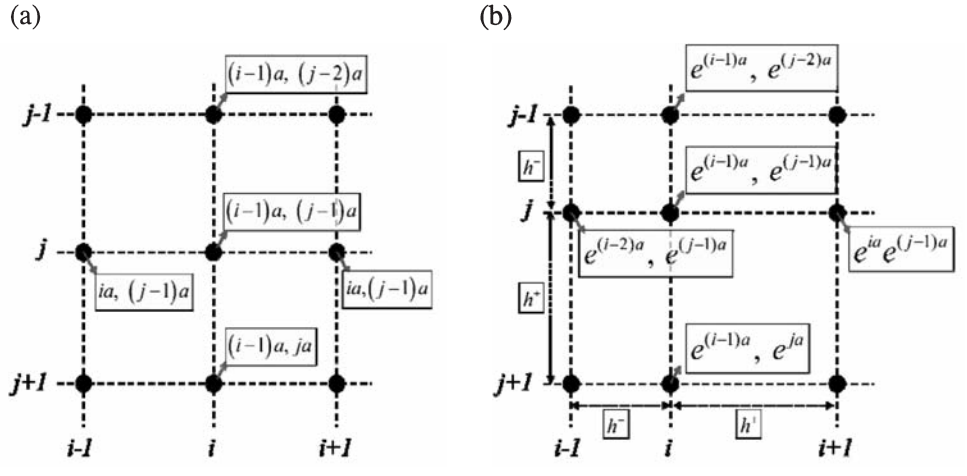

Fig. B-1. (a) Grid set where grid interval is uniform as 'a' in the logarithmic scale and (b) its corresponding grid set in the uniform scale where grid interval increases exponentially.

The second-order partial derivative terms in 2D acoustic and elastic wave equations can be discretized as

$$\partial^2 u/\partial x^2 = (\partial/\partial x)(\partial u/\partial x)$$

$$\approx \{[(u_{i+1,j}-u_{i,j})/h^+] - [(u_{i,j}-u_{i-1,j})/h^-]\}/[(h^+ + h^-)/2]$$

$$= [2/(h^-)^2]\{[(u_{i+1,j}-u_{i,j}) - (u_{i,j}-u_{i-1,j})(h^+/h^-)]/[(h^+/h^-)+1](h^+/h^-)\}$$

$$= [2/(h^-)^2]\{[(u_{i+1,j}-u_{i,j}) - (u_{i,j}-u_{i-1,j})e^a]/(e^a + 1)e^a\} \quad , \qquad \text{(B-1)}$$

$$\partial^2 u/\partial z^2 = [2/(h^-)^2]\{[(u_{i+1,j}-u_{i,j}) - (u_{i,j}-u_{i-1,j})e^a]/(e^a + 1)e^a\} \quad , \qquad \text{(B-2)}$$

$$\partial^2 u/\partial x \partial z = [2/(h^+ + h^-)][u_{i+1,j+1} - u_{i+1,j-1} - u_{i-1,j+1} - u_{i-1,j-1}] \quad . \qquad \text{(B-3)}$$

If we substitute the plane wave solutions $u_{i,j} = e^{-(i\omega t - ik_x x - ik_z z)}$, into eqs. (B-1) to (B-3), we obtain

$$\partial^2 p/\partial x^2 \approx [2/(h^-)^2]\{[(e^{ik_x h^+}-1) - (1-e^{-ik_x h^-})]/(e^a+1)e^a\}e^{-(i\omega t - ik_x x - ik_z z)} \quad ,(B\text{-}4)$$

$$\partial^2 p/\partial z^2 \approx [2/(h^-)^2]\{[(e^{ik_z h^+}-1) - (1-e^{-ik_z h^-})]/(e^a+1)e^a\}e^{-(i\omega t - ik_x x - ik_z z)} \quad ,(B\text{-}5)$$

$$\partial^2 p/\partial x\partial z \approx [2/(h^-)^2(e^a+1)^2]\begin{bmatrix} e^{ik_x h^+}e^{ik_z h^+} - e^{ik_x h^+}e^{-ik_z h^-} \\ -e^{-ik_x h^-}e^{ik_z h^+} + e^{-ik_x h^-}e^{-ik_z h^-} \end{bmatrix} e^{-(i\omega t - ik_x x - ik_z z)} . \quad (B\text{-}6)$$

The normalized phase velocity can be expressed as follows:

$$c_{ph}/c = (\omega/k)/c = (1/kh^-)\sqrt{(Axx + Azz)}$$

$$= [1/(2\pi/G)]\sqrt{(Axx + Azz)} \quad , \qquad (B\text{-}7)$$

$$Axx = -2\{[(e^{ikcos\theta h^+} - 1) - (1 - e^{-ikcos\theta h^-})e^a]/(e^a + 1)e^a\} \quad , \qquad (B\text{-}8)$$

$$Azz = -2\{[(e^{iksin\theta h^+} - 1) - (1 - e^{-iksin\theta h^-})e^a]/(e^a + 1)e^a\} \quad , \qquad (B\text{-}8)$$

for 2D acoustic wave equation, and

$$\alpha_{ph}/\alpha = (\omega/k_p)/\alpha$$

$$= (1/k_p h^-)\sqrt{\{\tfrac{1}{2}[1 + (\beta^2/\alpha^2)](Exx + Ezz)$$

$$+ \tfrac{1}{2}[1 - (\beta^2/\alpha^2)]\sqrt{[(Exx - Ezz)^2 + 4(Exz)^2]}\}$$

$$= [1/(2\pi/G_s)(\beta/\alpha)]\sqrt{\{\tfrac{1}{2}[1 + (\beta^2/\alpha^2)](Exx + Ezz)$$

$$+ \tfrac{1}{2}[1 - (\beta^2/\alpha^2)]\sqrt{[(Exx - Ezz)^2 + 4(Exz)^2]}\} \quad , \qquad (B\text{-}10)$$

$$\beta_{ph}/\beta = (\omega/k_s)/\beta$$

$$= (1/k_s h^-)\sqrt{\{\tfrac{1}{2}[1 + (\alpha^2/\beta^2)](Fxx + Fzz)$$

$$+ \tfrac{1}{2}[1 - (\alpha^2/\beta^2)]\sqrt{[(Fxx - Fzz)^2 + 4(Fxz)^2]}\}$$

$$= [1/(2\pi/G_s)]\sqrt{\{\tfrac{1}{2}[1 + (\alpha^2/\beta^2)](Fxx + Fzz)$$

$$+ \tfrac{1}{2}[1 - (\alpha^2/\beta^2)]\sqrt{[(Fxx - Fzz)^2 + 4(Fxz)^2]}\} \quad , \qquad (B\text{-}11)$$

$$Exx = -2\frac{\left[\left(e^{ik_p \cos\theta h^+} - 1\right) - \left(1 - e^{-ik_p \cos\theta h^-}\right)e^a\right]}{\left(e^a + 1\right)e^a}$$

$$= -2\frac{\left[\left(e^{ik_s \frac{\beta}{\alpha} \cos\theta h^+} - 1\right) - \left(1 - e^{-ik_s \frac{\beta}{\alpha} \cos\theta h^-}\right)e^a\right]}{\left(e^a + 1\right)e^a}, \quad \text{(B-12)}$$

$$Ezz = -2\frac{\left[\left(e^{ik_s \frac{\beta}{\alpha} \sin\theta h^+} - 1\right) - \left(1 - e^{-ik_s \frac{\beta}{\alpha} \sin\theta h^-}\right)e^a\right]}{\left(e^a + 1\right)e^a}, \quad \text{(B-13)}$$

$$Exz = \frac{1}{\left(e^a + 1\right)^2}\begin{bmatrix} e^{ik_s \frac{\beta}{\alpha} \cos\theta h^+} e^{ik_s \frac{\beta}{\alpha} \sin\theta h^+} - e^{ik_s \frac{\beta}{\alpha} \cos\theta h^+} e^{-ik_s \frac{\beta}{\alpha} \sin\theta h^+} \\ -e^{-ik_s \frac{\beta}{\alpha} \cos\theta h^+} e^{+ik_s \frac{\beta}{\alpha} \sin\theta h^+} + e^{-ik_s \frac{\beta}{\alpha} \cos\theta h^+} e^{-ik_s \frac{\beta}{\alpha} \sin\theta h^+} \end{bmatrix}, \quad \text{(B-14)}$$

$$Fxx = -2\frac{\left[\left(e^{ik_s \cos\theta h^+} - 1\right) - \left(1 - e^{-ik_s \cos\theta h^-}\right)e^a\right]}{\left(e^a + 1\right)e^a}, \quad \text{(B-15)}$$

$$Fzz = -2\frac{\left[\left(e^{ik_s \sin\theta h^+} - 1\right) - \left(1 - e^{-ik_s \sin\theta h^-}\right)e^a\right]}{\left(e^a + 1\right)e^a}, \quad \text{(B-16)}$$

$$Fxz = \frac{1}{\left(e^a + 1\right)^2}\begin{bmatrix} e^{ik_s \cos\theta h^+} e^{ik_s \sin\theta h^+} - e^{ik_s \cos\theta h^+} e^{-ik_s \sin\theta h^+} \\ -e^{-ik_s \cos\theta h^+} e^{+ik_s \sin\theta h^+} + e^{-ik_s \cos\theta h^+} e^{-ik_s \sin\theta h^+} \end{bmatrix}, \quad \text{(B-17)}$$

for 2D elastic wave equations using the relationship $k_p = k_s\,(\beta/\alpha)$.

Normalized phase velocity curve for acoustic wave equation obtained for a = 1 is shown in Fig. B-2. For comparison, we also display the normalized phase velocity curve obtained for the conventional, uniform grid set in Fig. B-2. The normalized phase velocities for the conventional, uniform grid set can be computed using a = 0. From Fig. B-2, we note that the logarithmic grid set requires more number of grid points per wavelength than the conventional uniform grid set to keep the same level of numerical dispersion, because the grid interval increases with distance when a is not zero. Numerical dispersion in the logarithmic grid set is dependent on the value of a.

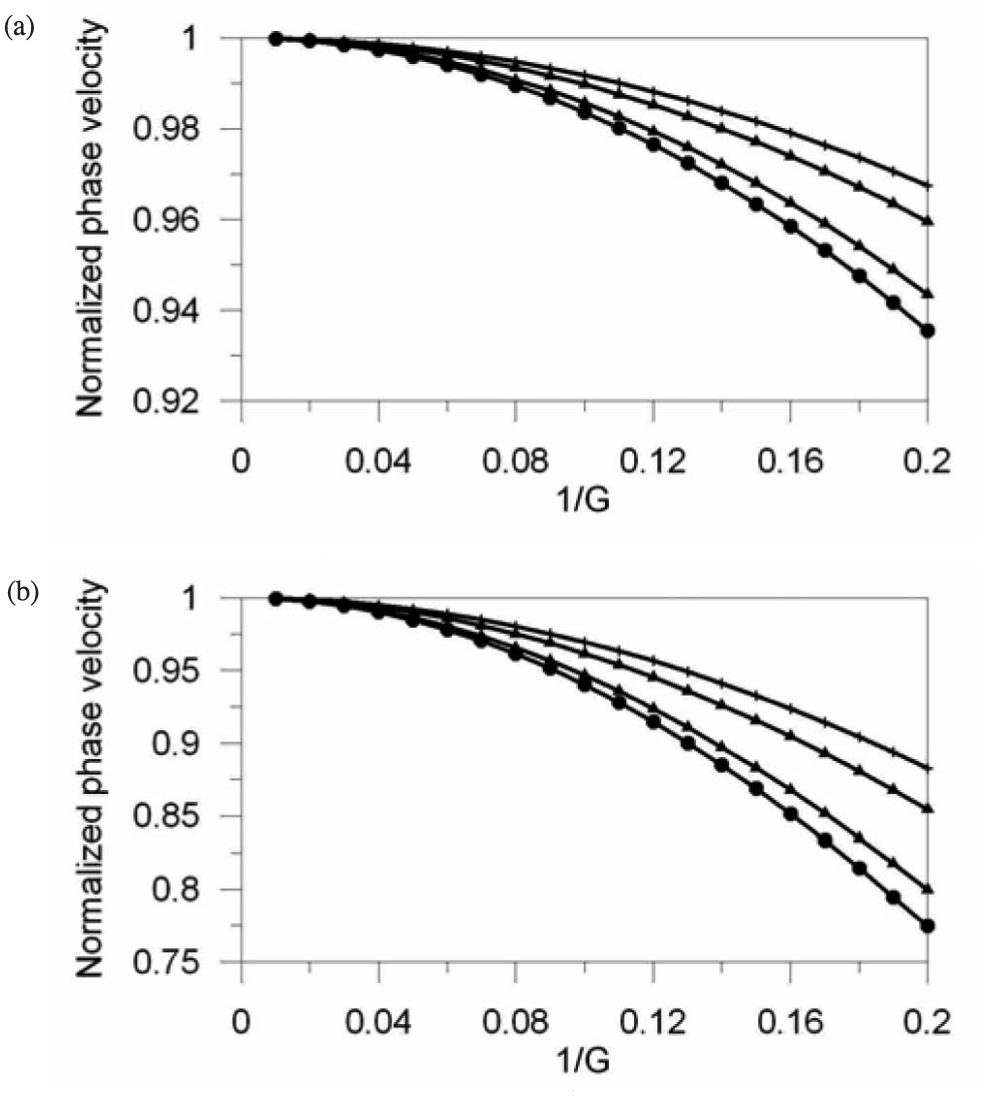

Fig. B-2. Dispersion curves for 2D acoustic wave equation in the (a) uniform and (b) logarithmic grid sets. In the logarithmic grid set, the grid interval increases with exponentially ($e^1 = 2.718$). G indicates the number of grid points per wavelength.

Figs. B-3 and B-4 show normalized P- and S-wave velocity curves, respectively, for elastic wave equation obtained for a = 1. We consider Poisson's ratios of 0.1, 0.2, 0.3 and 0.4. The overall patterns of numerical dispersion in the logarithmic grid set are similar to those of the conventional uniform grid set.

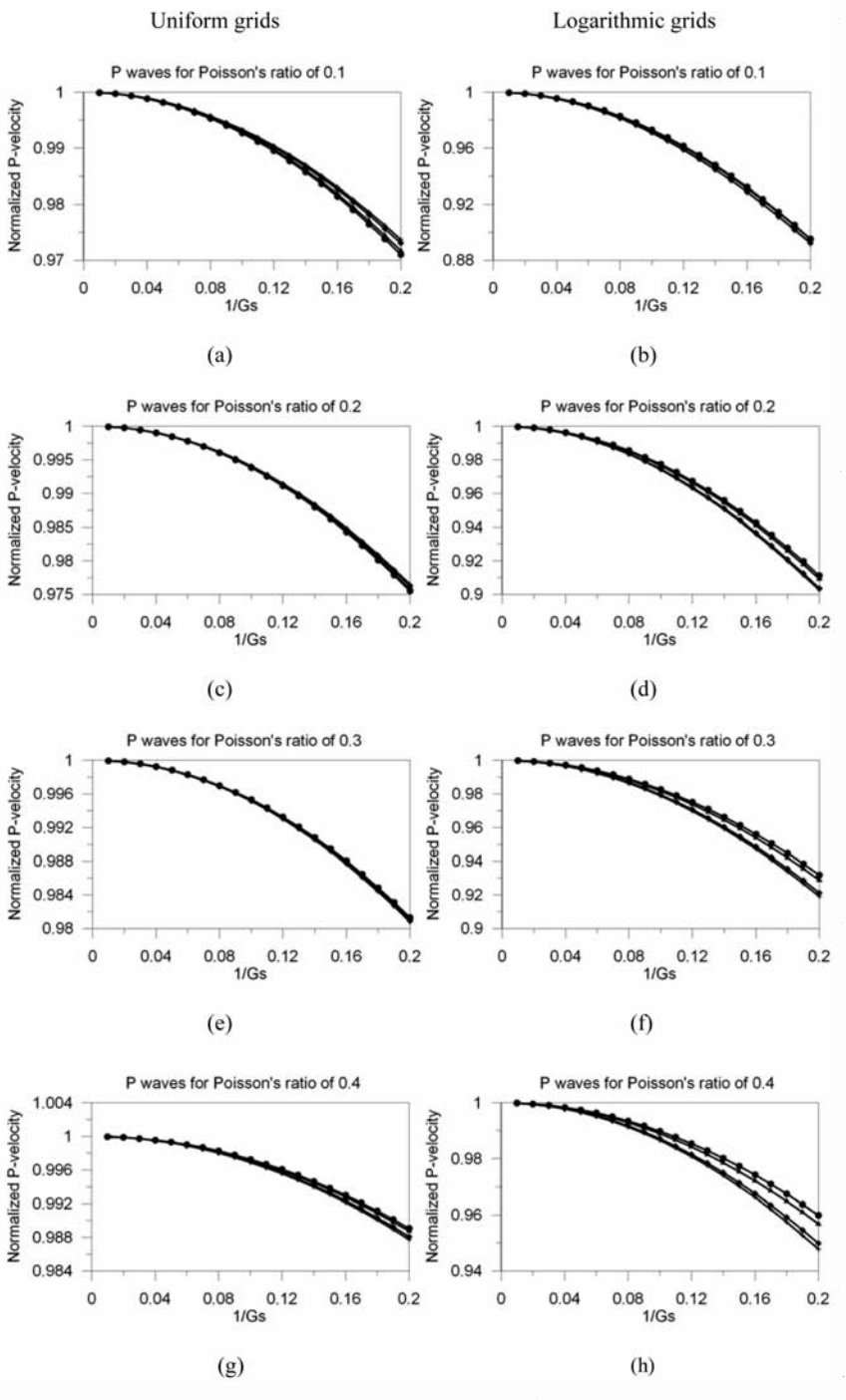

Fig. B-3. Dispersion curves for P waves of 2D elastic wave equation in the uniform (a, c, e, and g) and logarithmic (b, d, f, and h) grid sets, when Poisson's ratio is 0.1 (a and b), 0.2 (c and d), 0.3 (e and f), and 0.4 (g and h). In the logarithmic grid set, the grid interval increases with exponentially ($e^1 = 2.718$). Gs indicates the number of grid points per shear wavelength.

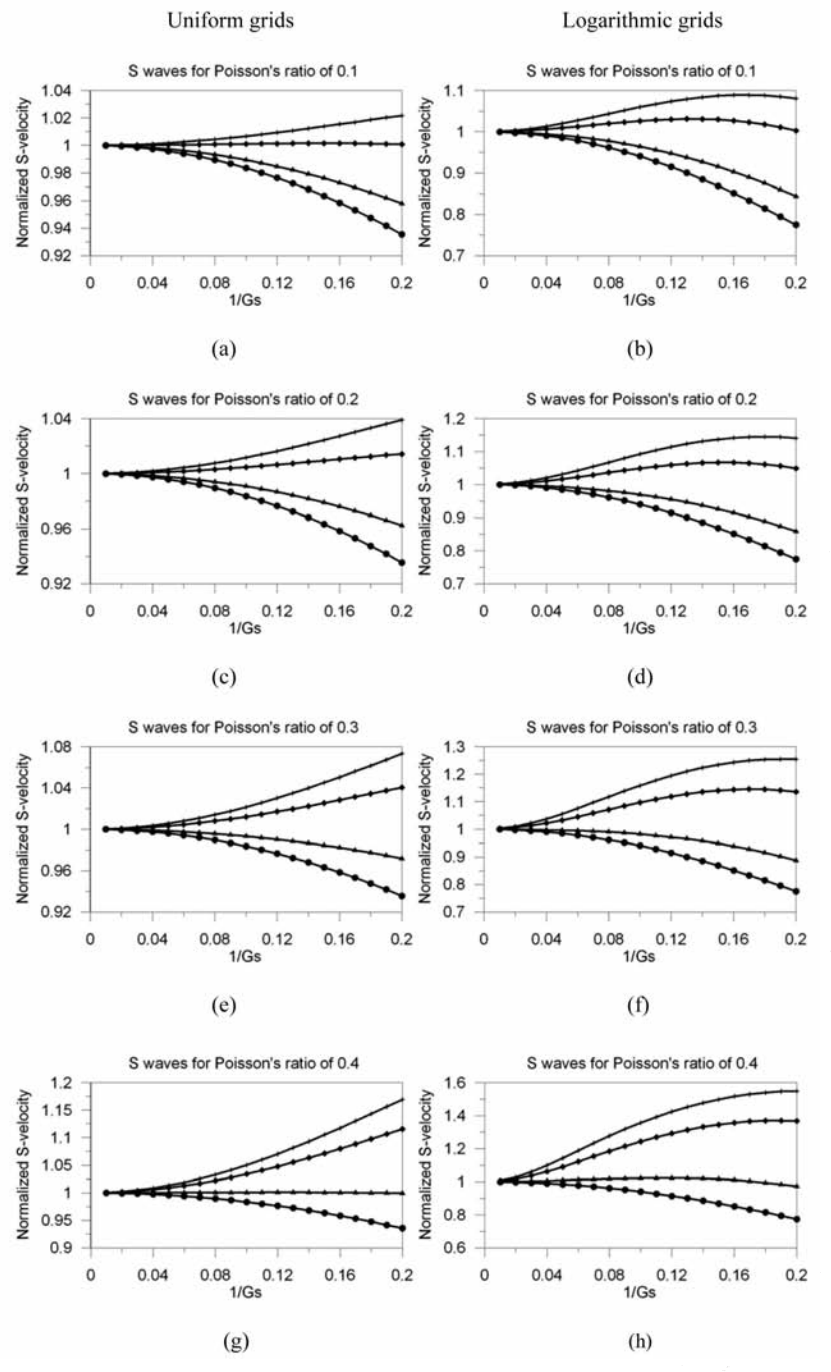

Fig. B-4. Dispersion curves for S waves of 2D elastic wave equation in the uniform (a, c, e, and g) and logarithmic (b, d, f, and h) grid sets, when Poisson's ratio is 0.1 (a and b), 0.2 (c and d), 0.3 (e and f), and 0.4 (g and h). In the logarithmic grid set, the grid interval increases with exponentially ($e^1 = 2.718$). Gs indicates the number of grid points per shear wavelength.